Spatial patterns of sound propagation in sand

Chu-heng Liu
The James Franck Institute and The Department of Physics, The University of Chicago, 5640 South Ellis Avenue, Chicago, Illinois 60637
(Received 18 November 1993; revised manuscript received 3 March 1994)

This paper addresses the problem of how sound propagates in a granular medium composed of noncohesive particles. This propagation has many unusual aspects which are due to the fragile nature of the contacts between grains. Sound propagation in a granular material is very sensitive to the exact position of each of the grains. The thermal expansion of a single bead of about 3000 Å can produce a change as large as 25% in the total transmission of the sound even though this expansion is 4 to 5 orders of magnitude smaller than the wavelength of the sound or the size of a bead (5 mm). I interpret this as being due to sound propagating predominantly along force chains within the medium. By replacing some of the beads with local heaters, I have used this effect to investigate the spatial properties of the low-amplitude vibrations. The disturbance of a single heater can be characterized by a time scale τ_h which reveals the elapsed time of the signal traveling along a path via the heater. Two heaters placed symmetrically with respect to the source and detector can produce very different disturbances. Finally, I show that the spatial pattern caused by heaters placed at different positions within the medium is very irregular in that two adjacent heaters can give very different responses. These experiments all indicate the presence of strong inhomogeneities and the existence of force chains within the medium along which the sound predominantly travels.

I. INTRODUCTION

Unconsolidated granular materials have very distinct properties that make them different from the other classes of conventional materials: gases, liquids, and solids.[1] For example, a pile of sand can have a nonzero slope showing that it can withstand external stresses as in a solid. However, if the slope becomes too large, the sand will start to flow similar to the behavior of a fluid. In saltation, quickly flowing sand can have mean free paths between collisions that are large compared to its diameter so that the material is reminiscent of a gas.

Sound propagation has been studied recently in an unconsolidated granular medium and was also shown to be very different from propagation in other media.[2,3] In sand, vibrations can propagate from one grain to its neighbors only through their mutual contacts if one neglects the interstitial fluid or gas. One can consider these contacts to be the building elements of the effective medium through which the sound travels. These contacts deform under pressure P with a very nonlinear form $\Delta \propto P^{2/3}$,[4] where Δ is the deformation of the bead at the contact. Several rather interesting phenomena were observed due to these disordered and nonlinear contacts. It was found that the frequency response characterizing the transmission spectrum is an interference pattern which is very irregular and configuration specific.[2] As the amplitude was increased, nonlinearity appeared near the onset of hysteretic behavior.[3] In the high-amplitude region, not only were fluctuations of the detected signal observed, but also frequency shifts in all of the structural features in the response were found.[2,3]

The apparent disorder in the packing of sand makes sound propagation reminiscent of wave phenomena in other disordered condensed-matter systems.[2,5,6] This analogy is made plausible since the frequency response of sound propagation in a sandpile has some features similar to conductance fluctuations seen in a mesoscopic metal.[7] With the assumption that this medium is homogeneous, diffusion wave theory or even localization theory may be relevant to the vibrational excitations in sand as was suggested by Feng and Sornette.[5]

This direct analogy may be flawed due to the unique properties of this unconsolidated material: the very fragile contacts between its constituent grains. For grains made of a hard material, the deformation Δ at a contact is extremely small compared to its grain size. Thus, one expects that a minute movement of a grain of sand comparable to Δ can effectively switch a sound propagation channel on or off, producing an extreme sensitivity of the vibration transmission to the exact spatial locations of the constituent particles. Such a sensitivity would be far greater than that found in other condensed-matter systems.

In the linear regime, the validity of the analogy to diffusive wave theory may be questionable due to another property unique to unconsolidated granular material which is related to the contacts: arching. Very slight disorder in the packing of the grains or a small spread in the distribution of the grain sizes could result in the formation of some very strong contacts as well as some very weak ones. Due to the equilibrium force balance within the pile, a strong contact is also likely to be followed by another strong one, thus leading to a chain of very strong contacts within the pile. Experiments in two dimensions[8] clearly support this picture: a few strong force chains support most of the external load. In three dimensions as well, there is experimental evidence for the existence of

such force chains.[9] If the strong contacts do exist and cluster into a dilute set of force chains, then the system will be inhomogeneous over a length scale considerably greater than the size of an individual bead. Consequently, the number of force chains along which sound preferentially travels would be so few that a diffusion description would not be justified. The past work on sound propagation in sand[1-3] has been primarily associated with only temporal aspects of this phenomena. However, spatial studies can be useful since they not only can reveal more information about sound which is not within the temporal description, but they can also provide some experimental evidence for the legitimacy of the analogy to diffusion.

In Sec. II, I will first briefly review and expand upon some of the previously studied temporal aspects of the low-amplitude vibration. Then in Sec. III, I discuss an effect in sand, namely that the thermal expansion of a single bead due to tiny changes in its temperature can significantly alter the transmission of sound. In the following section, I show how this effect can be used to investigate the spatial properties of the sound propagation. These measurements of the spatial properties are interpreted in terms of ballistic propagation along force chains and are thus in accord with the interpretation of the temporal behavior.

II. RESPONSE FUNCTION IN TIME AND FREQUENCY DOMAINS

In the experiments reported previously[2,3] and which I expand upon in this section, the granular material was composed of spherical glass beads with diameter $d=0.5$ cm. The beads were contained in a box with a 28 cm$\times$28 cm cross section and a depth ranging from 8 to 15 cm as shown in Fig. 1(a). The box was lined with Styrofoam sheets to reduce the reflection of the sound waves. Other layers of Styrofoam sheets and a plastic container enclosing the box protect the system from external vibrations and temperature fluctuations. The air surrounding the granular material was frequently refreshed with dry nitrogen to minimize the influence of humidity on the experiments. The source of the vibration was an aluminum disk 7 cm in diameter driven by a speaker via a horizontal rigid rod. An accelerometer attached to the back of the disk monitors the vibration and enabled control with good precision of the source amplitude through an electronic feedback loop. The detection accelerometers, 0.7 cm in diameter and 1.2 cm in length, are not sensitive to the acceleration in the transverse direction. They were placed 0.2–18 cm from the center of the source with their axes aligned along the direction of the source vibration. They were chosen to have a size comparable to that of a single glass bead so as to characterize the motion of the granular material down to the length scale of its constituent grains. Since both the glass beads and the detectors have very high density compared to air, their motion is affected little by the surrounding atmosphere.[2,3]

I first investigate the nature of sound propagation in the time domain. A pulse generated at the source arrives at the detector with a certain time delay and the clearest and most robust feature of this propagation process is the well-defined rising edge when the first effect of the source pulse is felt at the detector. The elapsed time for this rising edge to reach the detector yields a time-of-flight sound speed: $c_{\text{tof}}=280\pm30$ m/sec. Measurements in vacuum and in helium gas ($c=970$ m/sec) have excluded any possible contribution from the interstitial air ($c=330$ m/s). The response function $R(\tau)$ of the system has also been measured.[3] A short pulse at the source was generated and the vibration of the detector $D(\tau)$ was detected. Because this pulse could not be made arbitrarily short due to ringing in the speaker, the actual wave form of the source pulse was also recorded. The suitably filtered Fourier transform of the signal from the detector $D(\tau)$ was divided by that from the source. The ratio is the frequency response function $F(\nu)$, from which one can reconstruct the response in the time domain $R(\tau)$ by an inverse Fourier transform. In Figs. 1(b)–1(d) I show data for $R(\tau)$ for a detector at three distances $L_d=1$, 6, and 12 cm away from the source, respectively. Common features of these response functions are a sharp rising edge followed by a few strong spikes and a decaying tail.

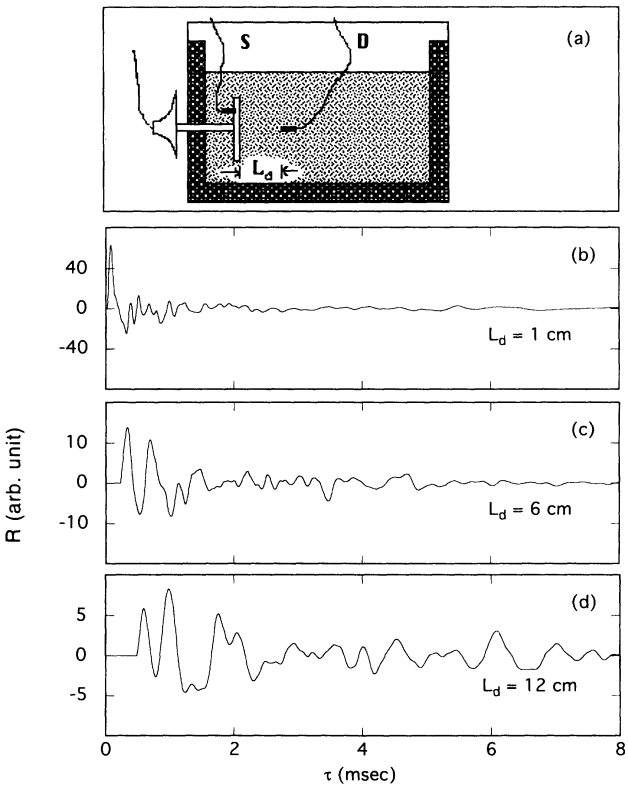

FIG. 1. (a) A schematic diagram of the side view of the experimental configuration. S and D correspond to the two accelerometers used to monitor the source acceleration and the detected signal, respectively. The walls are padded with 3-cm-thick sheets of Styrofoam. The response at the detector R as a function of elapsed time τ for three different source-detector distances as labeled in the figure. (b) $L_d=1$ cm; (c) $L_d=6$ cm; (d) $L_d=12$ cm. Data shown in (b), (c), and (d) have been calibrated with the same unit.

However, the structure of the response changes systematically with distance: At short distances, $R(\tau)$ is dominated by a sharp first peak with a small time delay between subsequent spikes. As L_d increases, the sharp features disappear and the contributions from longer times become more important.

The response function in the frequency domain $F(\nu)$ can be measured with higher precision by monitoring the detected signal as a function of frequency rather than a direct Fourier transform of $R(\tau)$. The source was driven with a single frequency ν: $A_s\sin(2\pi\nu t)$. The steady-state response of the detector also has the same frequency ν with the general form: $A_d\sin(2\pi\nu t+\phi)$, in which both A_d and ϕ are frequency dependent. Both the phase ϕ and the transmission $\eta=A_d/A_s$ of the complex frequency response $F(\nu)=\eta e^{i\phi}$ are shown versus the driving frequency ν in Figs. 2(a) and 2(b), respectively. Within experimental error, the phase is a linear function of frequency, implying that another velocity can be obtained: $c_g=2\pi L_d(d\nu/d\phi)$. This second velocity, measured by the phase delay, is the classical analogy of the group velocity. The value of c_g can vary within a range of 50–90 m/sec depending on the detailed packing of the grains. The transmission η has a rich and reproducible irregular pattern. If the pile is slightly disturbed, this fine structure can change and signify a new configuration. In Fig. 2(c), I show the response function $R(\tau)$ reconstructed from the frequency response data shown in Figs. 2(a) and 2(b). It is completely consistent with the $R(\tau)$ shown in Fig. 1(c) which has the same source-detector distance. The difference in the fine structure between these two curves demonstrates the slight difference in their packing configurations. The large difference between the group velocity c_g and the time-of-flight velocity c_{tof} is due to the wide range of time delays of the signals in $R(\tau)$. The interference between the signals at different time scales gives rise to the structure in the transmission function $\eta(\nu)$.

Besides the detailed structure in $\eta(\nu)$, the averaged overall transmission is of general interest since one can expect it to decay with both distance and frequency for several different reasons: the geometric factor due to the energy conservation; the attenuation due to inelasticity;[13] and the localization of the sound wave.[10] Figure 3(a) shows how the averaged transmission $\langle\eta\rangle_c$ varies against source frequency ν for the values of L_d labeled. The subscript c in the expression $\langle\eta\rangle_c$ denotes an average over different configurations. Figure 3(b) shows the variation of the transmission $\langle\eta\rangle_c$ versus the source-detector separation for different frequency bins. For all frequencies, the average transmission $\langle\eta\rangle_c$ decays exponentially with distance L_d. However, it was not possible to sort out the contributions to the signal decay from each of the three different physical processes just described.

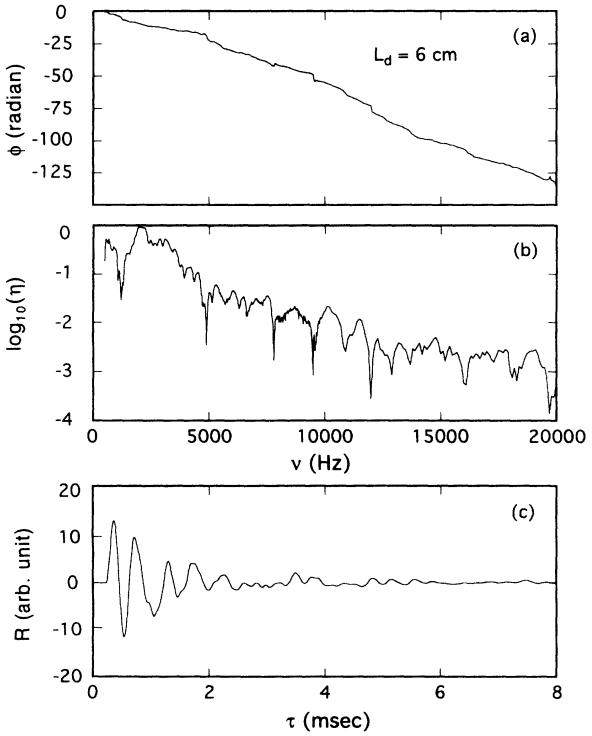

FIG. 2. The response function is presented in both frequency and time domain for a detector at a distance $L_d=6$ cm from the source. In (a) the phase ϕ and in (b) the transmission η are shown as a function of the source frequency ν. The slope of $\phi(\nu)$ determines c_g. In (c) the response R as a function of elapsed time τ is calculated from the data shown in parts (a) and (b).

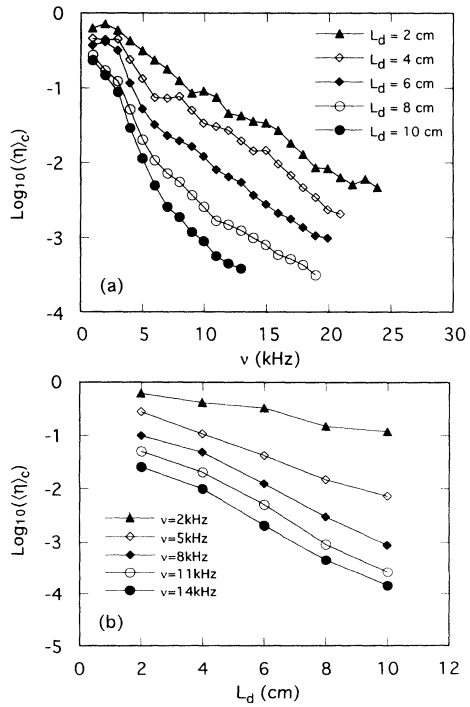

FIG. 3. (a) The averaged transmission response $\langle\eta\rangle_c$ is shown as a function of source frequency ν for five different source-detector distances as labeled in the figure. (b) The averaged transmission response $\langle\eta\rangle_c$ is shown as a function of source to detector distance L_d for five different source frequencies ν as labeled in the figure.

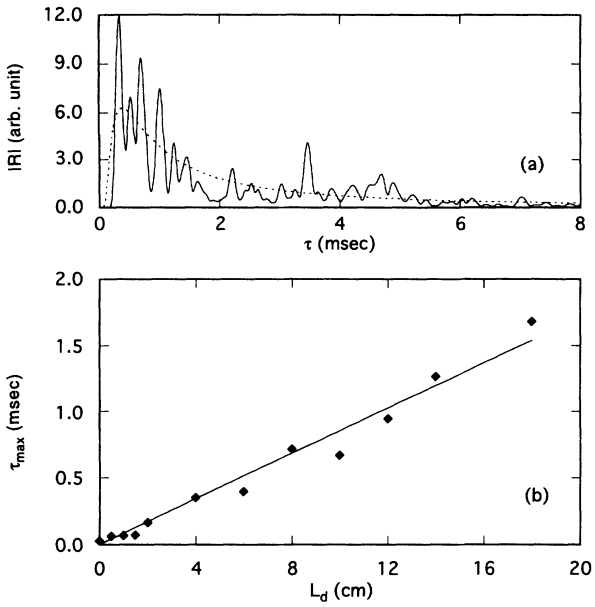

FIG. 4. (a) The absolute value of the response function $|R(\tau)|$ at $L_d=6$ cm is smoothed and then fit with a form appropriate for diffusion: $R(\tau)=a\tau^{-3/2}\exp(-b/\tau)$. (b) The elapsed time of the maximum response τ_{max} as a function of source detector separation L_d. The fit which is of the form $\tau_{max}=L_d/c$ yields a speed of sound $c=117\pm5$ m/s.

In order to understand the nature of these phenomena, one can first try to judge whether these vibrations are localized or extended. I estimate that the wavelength $\lambda=5.6$ cm for $c_{tof}=280$ m/s and a typical frequency $\nu=5$ kHz. With the assumption that the normalized mean free path l^* is of the order of the size of a bead, the Ioffe-Regel parameter[10] $kl^*\sim0.5$, which for a conventional system would have indicated that the system is close to the localization transition.[5] Diffusion-wave theory[11] may well apply to sound in sand in this regime.[5] Figure 4(a) shows the smoothed root-mean-square response at $L_d=6$ cm as well as a fit (the dotted line) to a function with a form which is appropriate for three-dimensional diffusion:[12] $R(\tau)=a\tau^{-3/2}\exp(-b/\tau)$ where a and b are fitting parameters. Figure 4(b) shows τ_{max} versus L_d, where τ_{max} is the time for the root-mean-square response to reach its maximum. These data extend to larger values of L_d than had been reported previously.[3] The data clearly favor a linear dependence and give rise to another speed $dL_d/d\tau_{max}=115\pm5$ m/s. Without absorption, the diffusion-wave theory is incompatible with our data. However, in the presence of absorption, the diffusion-wave model may account for this linear relation as pointed out by Sornette.[6]

III. FLUCTUATIONS AND DISTURBANCES DUE TO MINUTE MOVEMENTS

In this section I show that the contacts between grains are very fragile and show how this can be observed using either large-amplitude vibrations or using very small variations of temperature. In what I reported above, extreme care was taken to ensure the reproducibility of the response function within the experimental time scale. However, if one raises the amplitude of the source, the vibrations can become sufficiently intense that the contacts between beads may vary in time. With a source moving at constant frequency and amplitude, the vibration amplitude of the detector is very noisy. In Fig. 5(a), I show a time trace of the amplitude of the detector. As was seen in Ref. 2, over long times, the variation of the vibration amplitude is comparable to its mean value: $\delta A_d\sim\langle A_d\rangle$. Fluctuations are also present at shorter time scales. The power spectrum of these fluctuations shown in Fig. 5(b) indicates a power-law behavior: $S(f)\sim f^{-\alpha}$ with $\alpha\approx2.0$.[2,14,15] The power-law behavior persists over five decades in frequency and continues beyond the experimental time scale at the low-frequency end of the data. I have also noted that for the data in the figure, the amplitude is approximately 100 Å (for $\nu=4$ kHz and $A_s=0.71g$) for the displacement at the source. The essential length scale in this class of physical systems is most likely the deformation Δ of a bead at its contact which is estimated to be on the order of several hundred Å.[2,3] Therefore, even apparently small vibration amplitudes are likely to induce motion of the particles and therefore fluctuations in the transmitted signal.

As the source amplitude was lowered, small temperature changes within the container could dramatically change the response and dominate the observed fluctuations. For example, a temperature change of only 0.04 K in the pile caused by the ambient temperature drift in the room could cause a factor of 3 reversible change in the transmission, η.[2] The temperature dependence of the transmission is likely to be due to the thermal expansion of the glass beads since the beads have a thermal-expansion coefficient of about ~400 Å/K.

To further test this hypothesis and to check the limits of the sensitivity of the sound propagation to this perturbation, the response to a single local heater was measured.[16] This new setup differs from the previous one only by the addition of the heater (labeled H) embedded

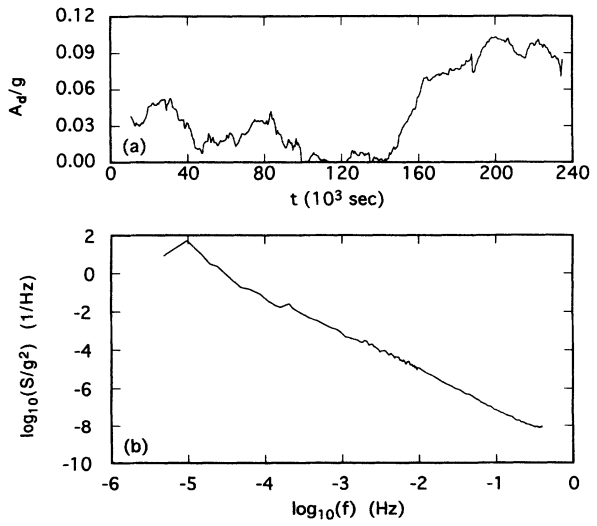

FIG. 5. (a) The time trace of the acceleration amplitude A_d, of a detector subjected to a source vibration $A_s=0.71g$ ($g=9.8$ m/s^2) at frequency $\nu=4$ kHz. (b) The power spectrum S of the fluctuations in A_d shown in (a).

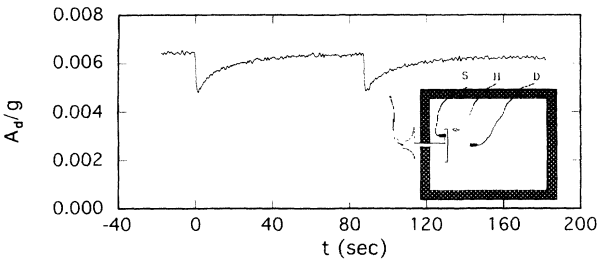

FIG. 6. The response of the amplitude of detector D to heat pulses sent to a heater. The two successive heat pulses at $t=0$ sec and $t=88$ sec each creates a thermal expansion $\Delta l \sim 3000$ Å. The source was run at a frequency $\nu=6.4$ kHz with an amplitude $A_s=0.14g$. This is the same set of data used in Ref. 16. Inset: a schematic diagram of the top view of the experimental apparatus. The heater is labeled H in the figure.

in the pile as shown in the inset of Fig. 6. The heater is a carbon resistor of approximately the same size as one of the glass beads with its surface smoothed. Figure 6 shows the time trace of the vibration amplitude of the detector, $A_d(t)$, during the course of which a brief current pulse was run through the resistor. As reported in Ref. 16, the amplitude of the detector drops suddenly during the application of the heat pulse. As the heat diffuses away, the signal returns to its original value with a time constant ~ 20 sec. I have shown that this is consistent with the time it takes for the temperature of the heater to recover as confirmed by a measurement of the temperature of the heater itself. The second pulse shown in Fig. 6 demonstrates the reproducibility of this effect.

In this measurement, each pulse sent to the heater raised its temperature by only 0.8 K, and produced a thermal expansion of only $\delta l=3000$ Å along its length and 1500 Å along its width. These pulses produced an abrupt 25% change in the signal as shown in the figure, even though the expansion of the heaters was many orders of magnitude smaller than either the size of a single grain (0.5 cm) or the wavelength of the sound (~ 4.4 cm for $\nu=6.4$ kHz and $c_{\text{tof}}=280$ m/s).

IV. SPATIAL PATTERNS OF SOUND PROPAGATION

A. Experimental setup

I will now show how one can use the extreme sensitivity of the sound propagation to local thermal expansions to explore the spatial extent of the vibrations. The heaters used in the experiments are made of 50-Ω carbon resistors, machined to an ellipsoidal shape with length 1 cm and diameter 0.5 cm. I made their shape and surface smoothness as close to those of the glass beads as possible so that they would not perturb the structure of the sandpile once imbedded within it. Thin wires (0.075 mm) were used as the electrical leads to further minimize the perturbation introduced by the heater array. Both the expansion and the temperature responses of the heater to an input current pulse can be characterized by a quick rise within the pulse duration and an exponential decay after the pulse with a time constant of about 20 sec. A typical pulse lasts 0.2 sec and the temperature takes about 2 sec to reach its maximum at the surface of a heater. Other measurements done in open air and in vacuum enabled us to understand the mechanism of this heat dissipation: roughly 40% of the heat is carried away by the neighboring beads through their contacts while the electrical leads and the surrounding air take away the remainder.

Figure 7 is a schematic diagram with the relative dimensions and locations of the heaters, the detectors and the source. Two detectors, placed in a line that is perpendicular to the center of the source, were at distances $L_{d1}=4.0$ cm and $L_{d2}=8.0$ cm away from the source. The heaters forming an eight row by six column array are horizontally place in a plane 1 cm below the level of the detectors and the center of the source. The precision of the heater placement is about 0.1 cm, since I could not accomplish more accurate positioning without forcing the sandpile to be packed in an unnatural way due to the discrete nature of the sand grains.

B. Response function to a single heater disturbance

The influence of the thermal expansion upon the vibration transmission does not always behave in the simple exponential fashion shown in Fig. 6. Figure 8 shows a rather complicated response to a pulse. The position of the heater is near the one used to produce Fig. 6, but the packing configuration has been changed. After the initial quick jump caused by the expansion of the heater, the signal varies in an irregular and unpredictable fashion. A simple exponential decay is clearly inappropriate even though the system eventually recovers its original value after a time comparable to that of the thermal diffusion. I have verified that these irregular structures in the intermediate time scales are also reproducible. I hypothesize

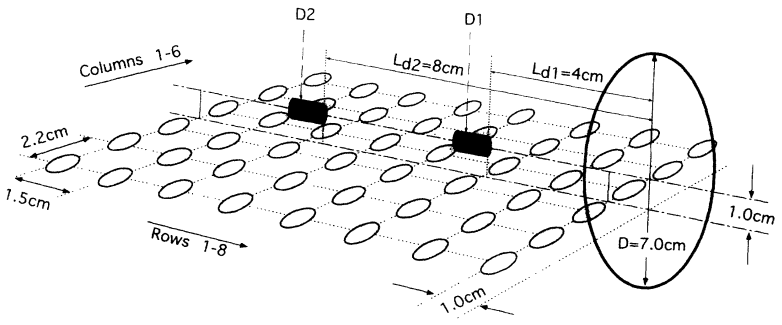

FIG. 7. A schematic diagram showing the relative locations of the heaters, the two detectors and the source. The large circle represents the source and the small shaded elliptical objects show the grid formed by the heaters. The heaters are identified by their row and column numbers. The two detectors labeled D1 and D2 are 4.0 and 8.0 cm away from the center of the source, respectively, and are 1 cm above the plane of the grid of the heaters.

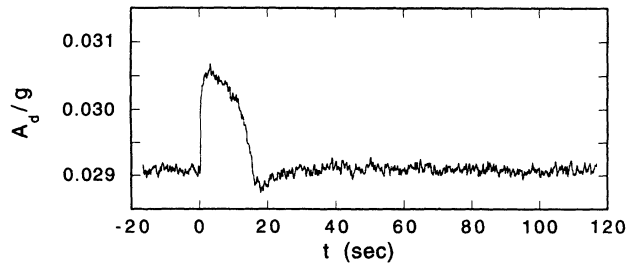

FIG. 8. The time trace of the vibration amplitude of the detector D1 due to a heat pulse in heater R8C2. The heat pulse sent in at $t=0$ creates a thermal expansion $\Delta l \sim 3000$ Å. The corresponding source vibration is at a frequency $\nu=5.5$ kHz with an amplitude $A_s=0.14g$.

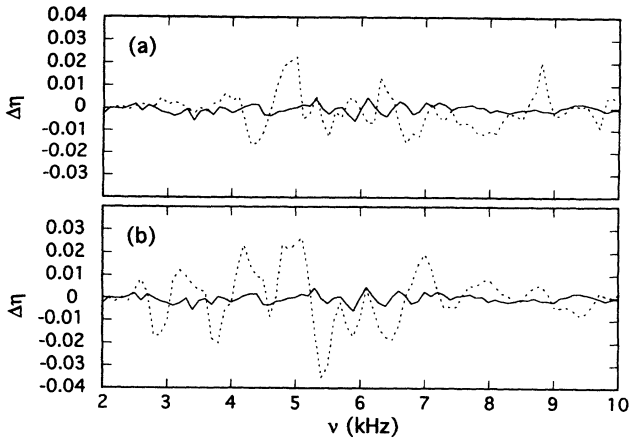

FIG. 9. The change in the transmission, $\Delta\eta$, of detector D1, caused by the thermal expansion $\Delta l=3000$ Å of a heater, plotted as a function of source frequency. (a) The solid and dotted line show $\Delta\eta$ caused by two symmetric heaters R8C2 and R8C4 in a single packing configuration. (b) The solid and dotted lines show the $\Delta\eta$ corresponding to two different packing configurations for the same heater R8C2.

that the time trace in Fig. 6 corresponds to a configuration such that the heater happens to be in a major force chain, and that the expansion of the heater itself dominates the response. In the case shown in Fig. 8, I argue that the heater's expansion has less effect on the sound transmission than do the expansions of its neighbors. Therefore, when the heat diffuses to its neighbors during the time of the measurement, a rather complicated response is produced.

I have demonstrated that the change in the transmission immediately after a heat pulse is directly related to the expansion of the heater, since one can separate this time scale (0.2 sec) from that of the expansion of its neighbors (greater than 1 sec) and that of thermal diffusion ($\sim$20 sec). In order to measure this abrupt change caused by the expansion of the heater alone with good signal to noise ratio, I have measured the time trace of the detector's vibration amplitude 10 sec before and after the heater pulse and fit both time traces with a quadratic form. The discontinuity between the two extrapolated values at the instant when the pulse is produced is taken as the direct effect of the heater's expansion. In all of our measurements, each heat pulse lasting 0.2 sec raises the temperature of a heater by 0.8 K and produces an expansion of 3000 Å in the longitudinal direction of the heater. I drive the heaters with current pulses 11 sec apart to speed up the measurements, which implies that a second pulse is sent in even before the system completely recovers (which takes over 20 sec) from the influence of the previous pulse. The justification of this measurement depends on the fact that the time scale of the pulse is much shorter than that of the secondary thermal effect. Measurements done with longer time intervals produce fully consistent results. The source amplitudes have been kept small enough to be within the linear regime such that one can generalize the change of the detector's vibration ΔA_d in terms of the change in the response function $\Delta\eta$.

To elucidate the implication of these abrupt changes in the system's response function, I show, in Fig. 9(a), the transmission change $\Delta\eta$ for two symmetric heaters R8C2 and R8C4 in the frequency range 2–10 kHz. Both measurements were carried out in an identical configuration of the beads. The disturbances are strong functions of the source frequency ν and they are reproducible. Due to the oscillating nature of the transmission change with source frequency ν, $\Delta\eta$ at a single frequency does not faithfully reveal the strength of the disturbance. However, one can still conclude that on average the heater R8C4 has a much greater effect than its symmetric counterpart R8C2. With a large enough frequency range one can measure the average strength of the disturbance caused by the expansion of any particular heater. Figure 9(b) shows the frequency dependence of the same heater R8C2 at a different configuration after the system has been disturbed (dotted line). The dotted line is different from the solid line not only in its peak (valley) frequencies but also in its overall magnitude. It is generally true for the data I have obtained that if a heater yields a strong (weak) disturbance in one particular configuration, the strong (weak) disturbances persist over the entire frequency range. This observation suggests that there is a common underlying mechanism (or path) that carries the signal for all frequencies from the source to the detector via the heater.

I note that there is a frequency scale $\Delta\nu$ over which there is a correlation in the disturbance in Fig. 9. The Fourier transform of this trace determines a time scale $\Delta\tau$. Roughly speaking, one can distinguish two types of heater disturbance based on the structure of the Fourier transform: one with a strong dominant peak (or set of closely spaced peaks) and the other with a noiselike spectrum. In Fig. 10, I show one typical data trace for each type. The corresponding self-correlation function and the power spectrum are also shown for each example. About 40% of the time there are clear periodic oscillations in the self-correlation function with a frequency interval $\Delta\nu$ and a single strong peak at $\Delta\tau=1/\Delta\nu$ in the power spectrum. In another 40% of the time there are only a few (2 or 3) closely spaced peaks in the power spectrum. In only 20% of the time do I get situations of the

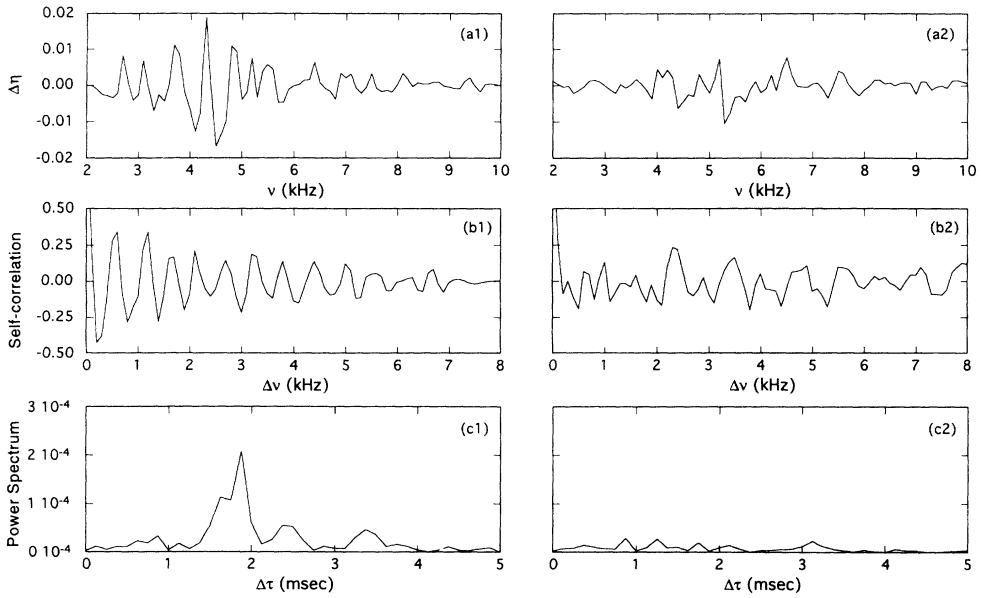

FIG. 10. (a1) and (a2) show two typical kinds of patterns of disturbance $\Delta\eta$ versus frequency ν. The data shown in (a1) and (a2) correspond to the disturbance to detector D1 caused by heaters R3C2 and R6C1, respectively. (b1) and (b2) show the corresponding self-correlation functions. (c1) and (c2) show the magnitude of the corresponding power spectra.

type shown in the second column of Fig. 10.

I argue that the oscillation of $\Delta\eta(\nu)$ is due to the interference between the signal carried by all the paths from the source to the detector (essentially the unperturbed situation) and the one that goes via the heater. Let us denote $R(\tau)$ and $\bar{R}(\tau)$ as the response function before and after the heater's expansion so that for each heater the quantity $R_h(\tau)\equiv\bar{R}(\tau)-R(\tau)$ is the disturbance to the response function caused by the expansion of the heater. In the frequency domain, $F_h(\nu)\equiv\bar{F}(\nu)-F(\nu)$ in which $F_h(\nu)$ is the Fourier transform of $R_h(\tau)$. Assuming that $\eta_h \ll \eta$ one can derive:

$$\begin{aligned}\Delta\eta&=\bar{\eta}(\nu)-\eta(\nu)\\&=|\eta(\nu)e^{i\phi(\nu)}+\eta_h(\nu)e^{i\phi_h(\nu)}|-\eta(\nu)\\&\approx\eta_h(\nu)\cos[\phi_h(\nu)-\phi(\nu)]\ ,\end{aligned}\tag{1}$$

in which $F_h\equiv\eta_h e^{i\phi_h}$ and $F\equiv\eta e^{i\phi}$. $\Delta\eta$ depends on both the amplitude of η_h and the phase difference $(\phi-\phi_h)$. This is consistent with the oscillating behavior of the results I have shown. Based on knowledge about the group velocity, one can explain the periodic structures seen in Fig. 10 (a1). The frequency dependence of the phase $\phi(\nu)$ in Fig. 2 (a) is $\phi(\nu)\approx 2\pi\nu\tau_g$, where τ_g is the time delay of the main signal corresponding to the "group velocity" c_g. If one assumes that there is a dominant time scale τ_h in $R_h(\tau)$, then $\phi_h(\nu)\approx 2\pi\nu\tau_h$ which implies that

$$\Delta\eta\approx\eta_h(\nu)\cos[2\pi\nu(\tau_h-\tau_g)]\ .\tag{2}$$

The frequency interval of the oscillation in $\Delta\eta$ is $1/|\tau_h-\tau_g|$ and the peak position in the power spectrum gives the value of $\Delta\tau_{\max}=|\tau_h-\tau_g|$. Since τ_g can be considered to be the collective delay of the main signal, τ_h can be interpreted as the delay of the signal as it travels from the source to the detector via the heater.

I argue that a heater which has the disturbance pattern of the type shown in Fig. 10 (a1) sits on one force chain which dominates all the other paths that go through the heater. From this one would expect that $\Delta\eta(\nu)$ has a single oscillation frequency. If two paths with comparable strength are disturbed at the same time by the heat pulse, then two frequency scales should show up. This would explain the multiple peaks in the power spectra that were often observed in the experiments. If the heater is outside of any strong force chains, then many time scales should come in with roughly equal strength as shown in Fig. 10 (a2).

The above analysis has shown that the disturbance caused by the heater expansion $F_h(\nu)\equiv\eta_h(\nu)e^{i\phi_h(\nu)}$ should really be considered as a vector in the complex plane. One can obtain both the parallel (in-phase with the main signal) and perpendicular (out-of-phase) components of $F_h(\nu)$ if one keeps track of the phase change $\Delta\phi\equiv\bar{\phi}-\phi$ as well as the transmission change $\Delta\eta$. In Figs. 11(a) and 11(b), I show both $\Delta\eta$ and $\Delta\phi$ of the detected signal respectively for a heater with a response of the type that gives several closely spaced peaks in the power spectrum. In Fig. 11(c), I show the in-phase (solid line) and the out-of-phase (dotted line) components of the same disturbance. The frequencies at which one of the two traces reaches a maximum or a minimum are just the frequencies at which the other trace crosses zero. This implies that these two responses are indeed 90° out of phase with each other. A diagram in Fig. 11(d) shows the relationship of these quantities with $\Delta\eta$ and $\Delta\phi$. Assuming $\eta_h \ll \eta$

$$\begin{aligned}(\eta_h)_{\parallel}&=\eta_h\cos(\phi_h-\phi)\\&=\bar{\eta}\cos(\Delta\phi)-\eta\\&=(\eta+\Delta\eta)\cos(\Delta\phi)-\eta\approx\Delta\eta\ ,\\(\eta_h)_{\perp}&=\eta_h\sin(\phi_h-\phi)\\&=(\eta+\Delta\eta)\sin(\Delta\phi)\approx\eta\Delta\phi\ .\end{aligned}\tag{3}$$

The close agreement between the solid line of Fig. 11(c) and that shown in Fig. 11(a) demonstrates the validity of this approximation. In principle, the sign of $\Delta\phi$ determines whether the parallel component is leading or trailing the phase of the perpendicular component by 90°. From this one can derive the sign of $\tau_h - \tau_g$. In most of the experiments, τ_h is clearly larger than τ_g, and I was not able to find a single case in which τ_h is significantly shorter than τ_g.

C. Spatial patterns of heater disturbances

I now turn attention to the spatial pattern of disturbance caused by the heater array. Figure 12 (a) plots the change in transmission $\Delta\eta$ for the array of heaters at frequency $\nu = 5$ kHz. A spike going up (down) implies that the pulse sent to that heater raised (lowered) the signal at detector D2 by an amount proportional to the height of the spike. The spatial pattern is very inhomogeneous and irregular in that two adjacent heaters can produce different effects. This seemingly unpredictable pattern is nevertheless reproducible. The data plotted in Fig. 12(b)

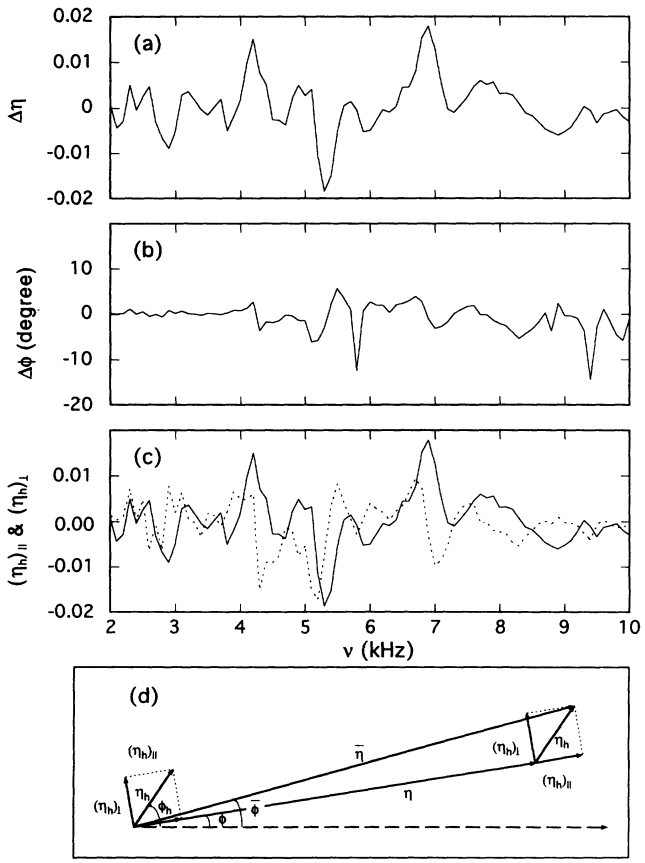

FIG. 11. The changes in the transmission $\Delta\eta$ and phase $\Delta\phi$ of detector D1 caused by the thermal expansion of heater R8C2 are shown in (a) and (b), respectively. In (c) the in-phase component (solid line) and the out-of-phase component (dotted line) of the heater disturbance function are shown as functions of frequency. (d) A schematic diagram shows the geometric relationship between the several measured and calculated quantities.

were taken immediately after that shown in (a) and shows a strong similarity to it. If I disturbed the sand even slightly, the pattern is completely changed as shown in Fig. 12(c). Just as the frequency response pattern shown in Fig. 2 can be considered a "fingerprint" of the precise configuration in the temporal domain, this disturbance pattern can be considered the corresponding signature in space.

The fact that the spatial correlations of $\Delta\eta$ disappear completely at a distance scale of the heater separation is evident from Fig. 12. This can also be explained by the force chain model. The expansion of a bead within a force chain could strengthen the connection and consequently increase the transmission. If a bead next to a force chain expands, it could exert a transverse stress on the chain, thereby weakening the connection and giving rise to a completely different response. The patterns in Fig. 12 have both amplitude and phase information and cannot be simply interpreted as the chain pattern. I was unable to obtain spatial patterns from one single configuration at many frequencies due to the intrinsic fluctuations caused by the source vibration itself and the ambient temperature drift. However, one can compare the disturbance strengths of two heaters placed symmetrically with respect to the source and the detector and thus understand the inhomogeneity in the system. I ran current through two symmetric heaters one at a time and measured the root-mean-square disturbance over the frequency range from 2 to 10 kHz.

After subtracting the background noise from the data, I calculate a quantity which characterizes the inhomogeneity

$$X = \frac{|\langle \Delta\eta_1 \rangle_\nu - \langle \Delta\eta_2 \rangle_\nu|}{\langle \Delta\eta_1 \rangle_\nu + \langle \Delta\eta_2 \rangle_\nu} , \tag{4}$$

where $\langle \Delta\eta_{1,2} \rangle_\nu$ is the root-mean-square average of $\Delta\eta$ over the frequency range 2–10 kHz and the subscripts 1 and 2 label each of the two symmetric heaters. I discard the data points if $\langle \Delta\eta_1 \rangle_\nu$ and $\langle \Delta\eta_2 \rangle_\nu$ are both less than twice the magnitude of the noise so that such data will not contribute to the correlations. The quantity X can only vary within the range between 0 (if $\langle \Delta\eta_1 \rangle_\nu$ and $\langle \Delta\eta_2 \rangle_\nu$ differ by just a small amount) and 1 (if one of them is much stronger than the other). Figure 13 shows the probability distribution of X calculated from the data of 16 pairs of heaters. In the main plot, the center two columns of heaters were excluded in case there was any correlation between two neighboring columns. In the inset one sees that including all the columns does not change the qualitative shape of the distribution.

The distributions cover a wide range in X and show a shoulder in (a) and a peak in (b). Although the heavy statistical weight at small X is within common expectation, the wide distribution and the second peak around $x = 0.35$ is far from conventional. If one assumes a narrow peak distribution of the quantity $\langle \Delta\eta \rangle_\nu$ around the average value $\overline{\langle \eta \rangle_\nu}$ and picks two independent samples $\langle \Delta\eta_1 \rangle_\nu$ and $\langle \Delta\eta_2 \rangle_\nu$, the histogram of X should be peaked around $X = 0$. To illustrate this I also show in Fig. 13 the distribution of X assuming a Gaussian distri-

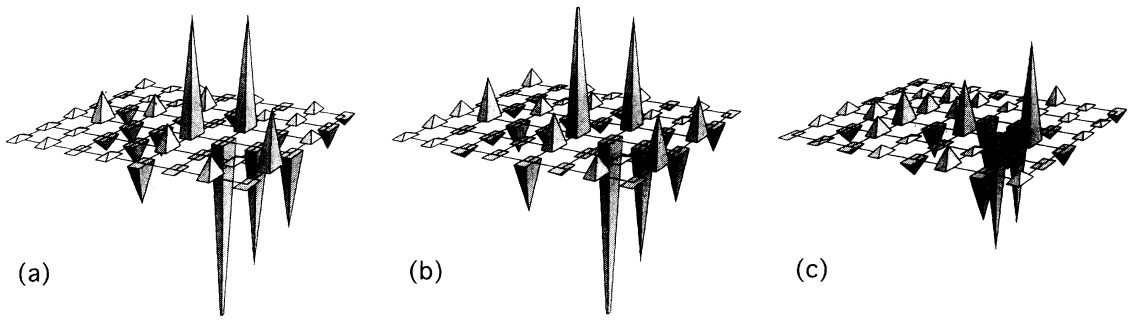

FIG. 12. (a) The spatial pattern of the disturbance to the transmission $\Delta\eta$ of detector D2 at a source frequency $\nu=5$ kHz. Each rectangle on the grid corresponds to a heater located at that grid and the height of each pyramid is proportional to $\Delta\eta$. (b) The same measurement as in (a) taken immediately after that of (a). (c) The same measurement as in (a) but with a slightly disturbed arrangement of the beads.

bution (dashed line) of $\langle\Delta\eta\rangle_\nu$ in which the mean $\overline{\langle\Delta\eta\rangle_\nu}$ is four times its standard deviation. It is clear that this distribution does not fit our data. The dominant contribution to the statistics near $X=0$ is due to a hypothesized narrow distribution of $\langle\Delta\eta\rangle_\nu$. One would have to choose a wide distribution of $\langle\Delta\eta\rangle_\nu$ in order to gain more weight at large X. By wide, I mean that the width of the distribution is comparable to its mean, which implies that $\langle\Delta\eta\rangle_\nu$ is very likely to be around zero. I show the distribution of X (dotted line) based on the two independent samples $\langle\Delta\eta_1\rangle_\nu$ and $\langle\Delta\eta_2\rangle_\nu$ from a hypothesized Rayleigh distribution of $\langle\Delta\eta\rangle_\nu$:

$$P(\langle\Delta\eta\rangle_\nu)=\frac{\pi\langle\Delta\eta\rangle_\nu}{2\overline{\langle\Delta\eta\rangle_\nu}^2}\exp\left[-\frac{\pi\langle\Delta\eta\rangle_\nu}{4\overline{\langle\Delta\eta\rangle_\nu}^2}\right] \tag{5}$$

the width of which $(1.05\overline{\langle\Delta\eta\rangle_\nu})$ is comparable to its mean. This generates a slightly more plausible fit to our data, but one which is still outside of experimental error. The shoulder structure in Fig. 13(a), and the peak at $X=0.35$ in Fig. 13(b), are still distinctively different from the fit. I note that a bimodal distribution of $\langle\Delta\eta\rangle_\nu$ could have a bimodal distribution of X. This is very suggestive in that $\langle\Delta\eta\rangle_\nu$ could have two modes, one strong and one weak, and consequently X would have a peak away from $X=0$. According to the peak position $X=0.35$, a strong disturbance is twice as effective as a weak one. However, this is unable to explain why the peak at $X\neq0$ is higher than the contribution near $X=0$. In this model, there was an implicit assumption that the two values of $\langle\Delta\eta\rangle_\nu$ were sampled independently. This assumption may be wrong. The force chains inside the pile may be so few that disturbances of two symmetric heaters cannot be considered as two independent samples from a common distribution.

The data plotted in Fig. 13 show the histogram of X taken from heaters at all positions. One would like to know whether this distribution still holds for a heater at a given position over many different packing configurations of the grains. In order to have enough statistics, one needs to sample many different configurations. I attempted to generate new configurations by driving the source at low frequency and high amplitude, or by intentionally changing the temperature. Although this process pro-

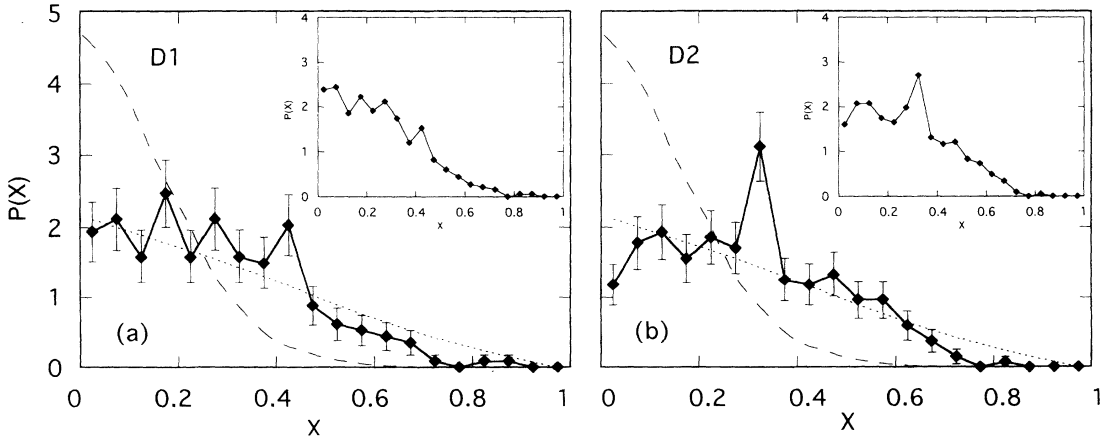

FIG. 13. The probability distribution function of quantity X, $P(X)$, calculated from data of the 16 pairs of symmetric heaters located at $C1, C2, C5$ and $C6$. (a) $P(X)$ for detector 1. (b) $P(X)$ for detector 2. Insets: The corresponding probability distribution functions $P(X)$ with the data from all 24 pairs of symmetric heaters included. The functions $P(X)$ calculated from independent sampling of some common distribution functions of $\langle\Delta\eta\rangle_\nu$ are also shown in the figure. Dashed line: a Gaussian distribution in which the mean is four times the standard deviation; Dotted line: $P(\langle\Delta\eta\rangle_\nu)=\pi\langle\Delta\eta\rangle_\nu/2\overline{\langle\Delta\eta\rangle_\nu}^2 \times\exp(-\pi\langle\Delta\eta\rangle_\nu/4\overline{\langle\Delta\eta\rangle_\nu}^2)$.

duces completely different disturbance patterns at individual frequencies as seen from Figs. 12(a) and 12(c), the root-mean-square strength of the disturbance pretty much remains unchanged. As I will discuss below, this suggests that a larger perturbation of the packing is needed in order to disturb the strength correlation.

I hypothesize that this more robust correlation in the strength of a heater disturbance is also due to the existence of force chains. In order to generate a different pattern at an individual frequency, the change in the phase of the disturbance of the order of π is enough. This can be easily achieved by the motion of the glass beads which do not belong to any strong force chains. However, the strong chains are more stable against mechanical disturbances. Other experiments investigating the nonlinear behavior of the transmission[3] lead to similar conclusions. I observed that loose particles rearrange at small vibration amplitudes which give rise to hysteretic behavior, while the particles in a strong chain are less susceptible to vibrations. Since a large value of $\langle \Delta\eta \rangle_v$ is closely related to the existence of a nearby force chain, the value of $\langle \Delta\eta \rangle_v$ will not change significantly until the strong chains are disrupted.

I now focus on the frequency-dependent spatial features. Figure 14 shows the root-mean-square disturbance $\langle \Delta\eta(\nu) \rangle_c$ vs the source frequency ν at a number of different distances. The subscript in the expression $\langle \Delta\eta(\nu) \rangle_c$ stands for the average over many configurations. Heaters far from the source predominantly perturb the lower frequency vibrations. For heaters closer to the source, the predominant perturbation is to those vibrations with higher frequencies. Intuitively one might argue that the change in the signal should depend on the strength of the vibration that reaches the heater itself since if no force chain carries the sound via the heater, its expansion cannot disturb the vibrations reaching the detector. As shown in Fig. 3, the transmitted signal decays strongly with distance and increasing frequency. A low-frequency signal can travel a long distance without much attenuation and hence can dominate the response of heaters far away. As the heater gets closer to the source, high-frequency components play a more important role.

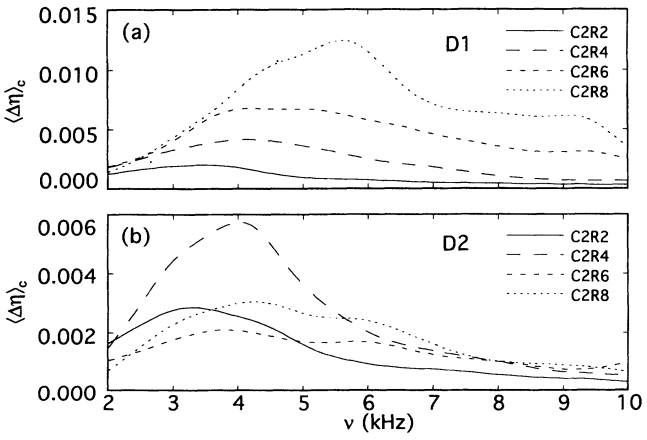

FIG. 14. The root-mean-square average of $\Delta\eta$ over many configurations $\langle \Delta\eta \rangle_c$ is smoothed and plotted versus the source frequency ν for a number of selected heaters as labeled in the figure. (a) and (b) correspond to detector D1 and D2, respectively.

Figure 15 shows the spatial variations of the root-mean-square $\langle \Delta\eta \rangle_c$ disturbances for several source frequencies ν. The data for detector D1 have an essentially monotonic variation with distance from the source, while the data for detector D2 show a strong peak at the positions close to the detector. The shorter the distance between the heater and the detector, the stronger the heater disturbance will be. I speculate that this is due to the perturbation of the structure surrounding the detector. As the heater gets closer to the detector, it can disturb a larger percentage of the paths that run between the source and the detector. This suggests another relevant length scale aside from the distance of the source to the heater L_{SH}, namely the distance from the heater to the detector L_{HD}.

When one makes a three-dimensional plot of $\log_{10}(\langle \Delta\eta \rangle_c)$ versus $\log_{10}(L_{SH})$ and $\log_{10}(L_{HD})$ for each detector at a single frequency, one finds that all the data points appear to fall in a plane. This implies that the data can be fit with a linear function of $\log_{10}(L_{SH})$ and $\log_{10}(L_{HD})$:

$$\log_{10}(\langle \Delta\eta \rangle_c) = -p1(\nu)\log_{10}(L_{SH}) - p2(\nu)\log_{10}(L_{HD}) + p3(\nu) . \quad (6)$$

Figure 16 shows $\log_{10}(\langle \Delta\eta \rangle_c) - p3(\nu)$ versus $-p1(\nu)\log_{10}(L_{SH}) - p2(\nu)\log_{10}(L_{HD})$ at three source frequencies $\nu = 3.5$, 6.5, and 9.5 kHz for detector D1. The data collapse onto the solid straight line. In Fig. 17, I show the dependence of these fitting parameters on ν. The parameters for both detector D1 (filled symbols) and detector D2 (open symbols) show qualitatively the same kind of behavior which implies that the dependence on ν is robust and not sensitive to the placement of the detectors. The exponent for the source-heater distance $p1$, increases monotonically with frequency, while the exponent for the heater-detector separation $p2$ appears independent of ν. Due to the limited precision of the measurements and the limited range of variation of the spatial coordinates, the data can also be well fit by another common form in which $\langle \Delta\eta \rangle_c$ decays with L_{SH} and L_{HD} in an exponential fashion. The parameters of the exponential fits show similar variations with frequency and the parameters for both detectors D1 and D2 are also in good agreement.

Finally, let us examine the spatial distribution of the time delays of the heater disturbance responses. As I have discussed earlier in Sec. IV B about 40% of the time there is a dominant frequency scale in $\Delta\eta$. The corresponding time scale $\Delta\tau_{max}$ is the difference between the effective time delay of the path that the heater disturbed, τ_h, and the time delay of the main signal, τ_g. Even in the case when there is no single dominant peak in the magnitude of the power spectrum of the heater disturbance, one can still obtain a range of $\Delta\tau_{max}$. I have observed that $\Delta\tau_{max}$ for a particular heater can have a wide distri-

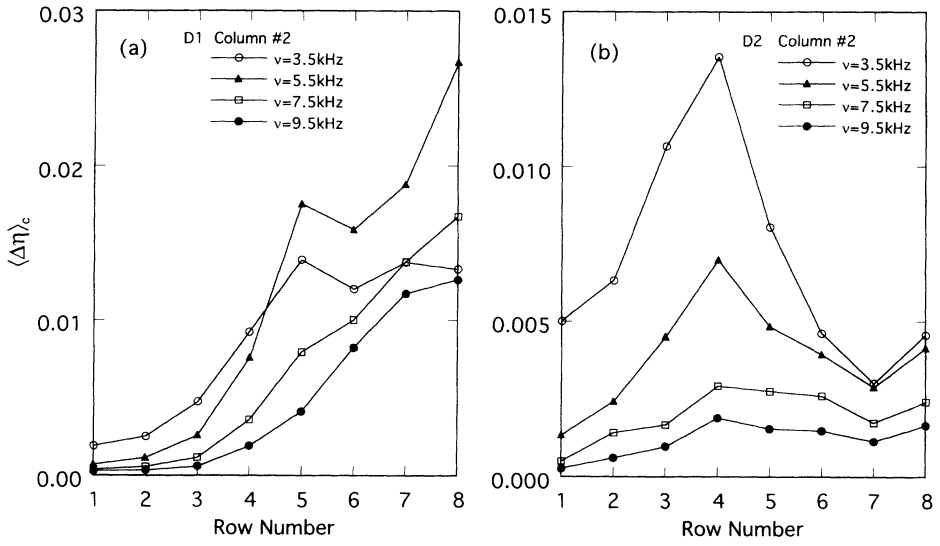

FIG. 15. The root-mean-square average of $\Delta\eta$ over many configurations $\langle\Delta\eta\rangle_c$ is binned and then plotted versus the heaters' spatial locations. The four curves are for four different frequency bins as labeled in the figure. (a) and (b) correspond to detector D1 and D2, respectively.

bution depending on the configuration of the grains. Over many configurations, the average shows a rather smooth variation with the spatial coordinates. Figures 18(a) and 18(b) show these time delays vs the spatial positions of detector D1 and D2, respectively. In general, this time delay increases as the heater moves farther away from either the source or the detector since the path is getting longer. According to the analysis in Sec. IV B, one can associate the time scale $\Delta\tau_{\max}$ that I measured with $\tau_h-\tau_g$ where $\tau_g=L_d/c_g$ is the time delay of the unperturbed signal and τ_h is the time delay along the disturbed path. Figure 18(c) plots $(\Delta\tau_{\max}+L_d/c_g)$ against the length of the shortest path connecting the source, heater and detector, $L_{\rm SH}+L_{\rm HD}$. Data points from both detectors collapse onto a straight line which implies a linear relation between τ_h and $L_{\rm SH}+L_{\rm HD}$. A one-parameter linear fit yields a slope corresponding to a speed of sound $c=50$ m/s, which is in excellent agreement with the group velocity c_g obtained from the phase part of the frequency response.

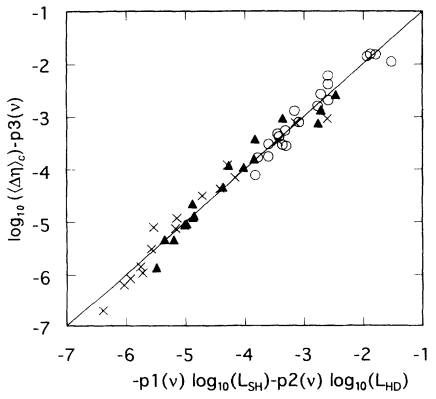

FIG. 16. The root-mean-square average of $\langle\Delta\eta\rangle_c$ over many configurations at a single frequency bin is fit with a power-law form $\langle\Delta\eta(\nu)\rangle_c=L_{\rm SH}^{-p1(\nu)}L_{\rm HD}^{-p2(\nu)}\times10^{p3(\nu)}$, where $L_{\rm SH}$ and $L_{\rm HD}$ are the distances from the heater to the source and the detector, respectively, and $p1(\nu)$, $p2(\nu)$, and $p3(\nu)$ are the fitting parameters. Data shown are for detector D1 at three source frequencies $\nu=3.5$ kHz (circle), 6.5 kHz (triangle) and 9.5 kHz (cross), respectively. The fit is the solid diagonal line.

V. CONCLUSIONS

In conclusion, I have studied the temporal and spatial properties of sound propagation in sand. The response function in time $R(\tau)$ has contributions with many different time scales. This wide distribution of times gives rise to not only the irregular patterns observed in the frequency response $\eta(\nu)$, but also to the slow sound

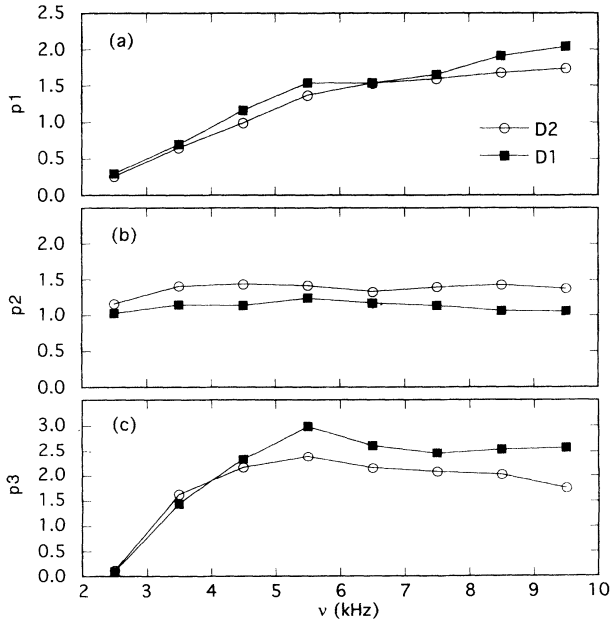

FIG. 17. The fitting parameters $p1(\nu)$, $p2(\nu)$, and $p3(\nu)$ of the power-law fit described in Fig. 16 are shown as functions of source frequency ν in (a), (b), and (c), respectively. The solid symbols are the fitting parameters for detector D1 and the open symbols are for detector D2.

speed $c_g = 60$ m/s measured from the phase delay which is the classical analogy of the group velocity. This group velocity is five times slower than the time-of-flight speed of sound $c_{tof} = 280$ m/s. An attempt to use a diffusion wave picture to explain the discrepancy between c_g and c_{tof} failed when I studied the distance dependence of the peak of the response function $R(\tau)$. It also failed when I analyzed the data from signals passing through heaters located at various positions. Both time scales show clear linear dependence on distance and seem to favor a model based on ballistic transport. It is interesting to note that diffusing waves in an absorptive medium could also give rise to a linear relation between time scale and distance within a limited range of distances.[6]

The fragile contacts between the glass beads have some important and unique consequences in many measurements which show extreme sensitivity to the detailed configuration of the packing. The detector vibration amplitudes can fluctuate with time at seemingly very low source vibration amplitudes of about 100 Å. Such fluctuations are large and have a power spectrum which obeys a power law over five decades in frequency: $S(f) \sim f^{-\alpha}$, with $\alpha = 2.0$. A small thermal expansion of a single heater can change the transmission by 25% even though this expansion is many orders of magnitude smaller than the wavelength of the sound or the diameter of the beads. Studies on the frequency dependence of the disturbance pattern reveals that the characteristic frequency interval $\Delta\nu$ in this pattern is directly related to the path-length difference between the main signal and the signal that has to move via the heater.

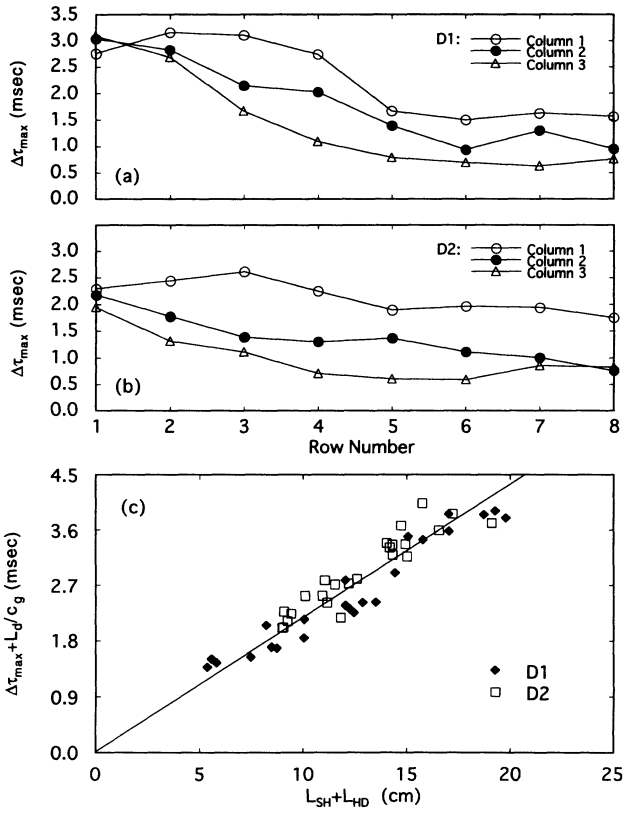

FIG. 18. The time of the peak response in Fig. 10(c), $\Delta\tau_{max}$, averaged over symmetric heaters and many configurations is plotted versus the spatial positions of the heaters. Different symbols are for heaters located at columns 1–3, respectively, as labeled in the figure. (a) shows the data for detector D1 and (b) shows the data for detector D2. (c) $\Delta\tau_{max}+L_d/c_g$ is plotted versus the length of the direct path along source-heater-detector $L_{SH}+L_{HD}$, where L_d/c_g is the time delay of the unperturbed signal. I used $c_g = 60$ m/s in these calculations. Open symbols are for detector D2 and solid ones are for detector D1. The one parameter linear fit to both the filled and open symbols yields a slope which gives rise to a speed of $c = 50$ m/s.

In conventional wave phenomena, the contribution due to the scattering by an individual particle is usually written as Fe^{ikx} in which F is treated as an intrinsic property of the particle. Such a formalism leads to the conclusion that Δx should be comparable to the wavelength λ in order to produce a significant effect on the scattered wave. However, in granular material, due to the small deformation at the interparticle contacts, the extremely sensitivity of F on x dominates the effect caused by the change in phase $e^{ik\Delta x}$.

Also as a consequence of the fragile contacts, the medium is very inhomogeneous. Measurements of the disturbance due to a heat pulse in many pairs of symmetric heaters clearly show a wide distribution of the chain strengths. The data suggest a bimodal structure in the distribution with two distinctive strengths: a strong one and a weak one. The heater disturbance measurements over many frequencies demonstrate that there are strong correlations in the response as a function of frequency, in both strength and phase. This suggests a common underlying mechanism, namely that the same set of paths are responsible for vibrations at all frequencies. This strong inhomogeneity of the medium, as well as the fact that the inhomogeneity persists despite small perturbations of the medium, is consistent with the force chain model: a small number of strong force chains carry most of the stress and the vibration.

This force chain structure is rather uncommon in other disordered condensed-matter systems and should be taken into account in studies of sound localization in this medium. Within the frequency range I have explored, the phenomenon of sound propagation in sand appears to be in a different regime than can be described by a diffusion-wave picture. It is possible that the observed nondiffusive behavior is due to the detector not being sufficiently far away from the source. The correlation length of the chain structure is also of vital importance since it may dominate the mean free path for the sound waves. The structure of the force chain network is currently under investigation.[9] Further studies of sound transmission in granular media with larger or smaller distances between the source and detector and at higher frequencies may reveal some features of diffusive waves and sound localization.

ACKNOWLEDGMENTS

I would like to thank H. Jaeger, T. Witten, J. Knight, N. Menon, R. Leheny, H. Li, C. Tang, X. D. Shi, D.

Weitz, and M. Leibig for many simulating discussions on various aspects of this work. I thank D. Sornette and S. Feng for sending their stimulating paper on using diffusion-wave theory to describe our results and their useful comments on our work. I would especially like to thank Professor Sidney Nagel, for motivating my interest in this subject and for his critical reading of this manuscript. This work was supported by the NSF Material Research Laboratory under Grant No. DMR-MRL 88-19860 and by DMR 91-11733.

[1]See, for example, H. M. Jaeger and S. R. Nagel, Science **255**, 1523 (1992), and references therein; *Disorder and Granular Media,* edited by D. Bideau and A. Hansen (North-Holland, Amsterdam, 1993); *Powder and Grains 93;* edited by C. Thornton (A. A. Balkema, Rotterdam, 1993); *Granular Matter,* edited by A. Mehta (Springer, Berlin, 1993).

[2]C.-h. Liu and S. R. Nagel, Phys. Rev. Lett. **68**, 2301 (1992).

[3]C.-h. Liu and S. R. Nagel, Phys. Rev. B **48**, 15 646 (1993).

[4]L. D. Landau and E. M. Lifshitz, *Theory of Elasticity* (Pergamon, New York, 1986), Chap. 1; J. Duffy and R. D. Mindlin, J. Appl. Mech. **24**, 585 (1957).

[5]S. Feng and D. Sornette, Phys. Lett. A **184**, 127 (1993).

[6]D. Sornette, J. Stat. Phys. **56**, 669 (1989).

[7]S. Washburn and R. Webb, Adv. Phys. **35**, 375 (1986); P. A. Lee and A. D. Stone, Phys. Rev. Lett. **55**, 1622 (1985); B. L. Al'tshuler, Pis'ma Zh. Eksp. Teor. Fiz. **41**, 530 (1985) [JETP Lett. **41**, 648 (1985)].

[8]See, T. Travers, M. Ammi, D. Bideau, A. Gervois, J. C. Messager, and J. P. Troadec, Europhys. Lett. **4**, 329 (1987), and references therein.

[9]C.-h. Liu, D. Schecter, S. R. Nagel, and R. Behringer (unpublished).

[10]*Scattering and Localization of Classical Waves in Random Media,* edited by P. Sheng (World Scientific, Singapore, 1990).

[11]D. J. Pine, D. A Weitz, P. M. Chaikin, and E. Herbolzheimer, Phys. Rev. Lett. **60**, 1134 (1988); G. Maret and P. E. Wolf, Z. Phys. B **65**, 409 (1987).

[12]This is the solution in three-dimensions to the equation $\partial R/\partial t = D\nabla^2 R$ with the initial condition that $R(t=0,r)=\delta(r)$. For d-dimensional diffusion: $R(\tau,r)=(4\pi D\tau)^{-d/2}\exp(-r^2/4D\tau)$.

[13]L. D. Landau and E. M. Lifshitz, *Theory of Elasticity* (Ref. 4), Chap. 5.

[14]In our previous paper (Ref. 2) we had quoted a value of 2.2 for the exponent. We are no longer convinced that the exponent is different from 2.0.

[15]M. Leibig, Phys. Rev. E **49**, 1647 (1994). Using a two-dimensional spring and point mass model with a random distribution of spring constants (or masses), Leibig has simulated some of these results, namely the patterns in Fig. 2(b) and Fig. 5.

[16]C.-h. Liu and S. R. Nagel, in *Proceedings of the 2nd Liquid Matter Conference, Firenze, Italy, 1993,* edited by J. P. Hansen, F. Barocchi, and V. Degiorgio [J. Phys. Condens. Matter (to be published)].

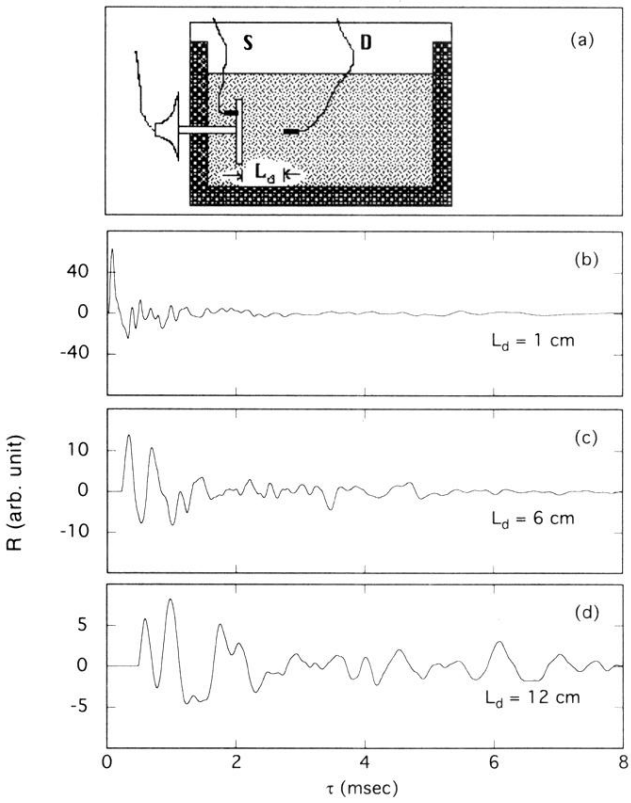

FIG. 1. (a) A schematic diagram of the side view of the experimental configuration. S and D correspond to the two accelerometers used to monitor the source acceleration and the detected signal, respectively. The walls are padded with 3-cm-thick sheets of Styrofoam. The response at the detector R as a function of elapsed time τ for three different source-detector distances as labeled in the figure. (b) $L_d = 1$ cm; (c) $L_d = 6$ cm; (d) $L_d = 12$ cm. Data shown in (b), (c), and (d) have been calibrated with the same unit.

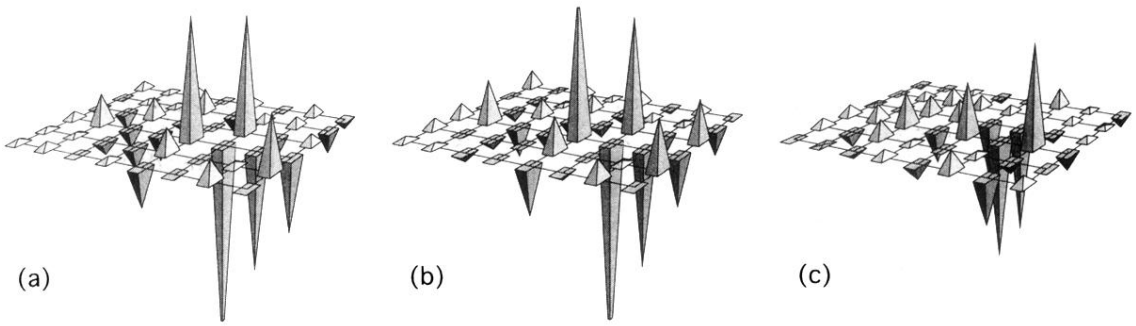

FIG. 12. (a) The spatial pattern of the disturbance to the transmission $\Delta\eta$ of detector D2 at a source frequency $\nu=5$ kHz. Each rectangle on the grid corresponds to a heater located at that grid and the height of each pyramid is proportional to $\Delta\eta$. (b) The same measurement as in (a) taken immediately after that of (a). (c) The same measurement as in (a) but with a slightly disturbed arrangement of the beads.

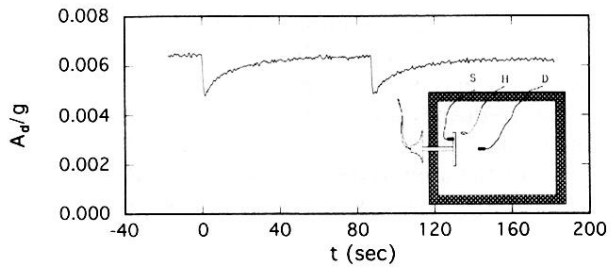

FIG. 6. The response of the amplitude of detector D to heat pulses sent to a heater. The two successive heat pulses at $t=0$ sec and $t=88$ sec each creates a thermal expansion $\Delta l \sim 3000$ Å. The source was run at a frequency $\nu=6.4$ kHz with an amplitude $A_s=0.14g$. This is the same set of data used in Ref. 16. Inset: a schematic diagram of the top view of the experimental apparatus. The heater is labeled H in the figure.

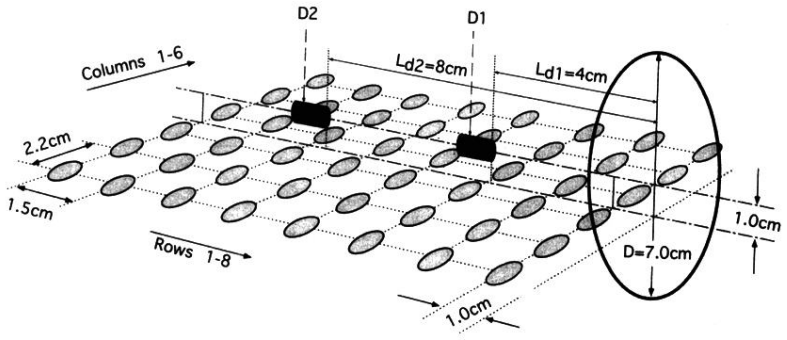

FIG. 7. A schematic diagram showing the relative locations of the heaters, the two detectors and the source. The large circle represents the source and the small shaded elliptical objects show the grid formed by the heaters. The heaters are identified by their row and column numbers. The two detectors labeled D1 and D2 are 4.0 and 8.0 cm away from the center of the source, respectively, and are 1 cm above the plane of the grid of the heaters.